
Variance-Covariance Regularization Enforces Pairwise Independence in Self-Supervised Representations

Grégoire Mialon¹ Randall Balestriero¹ Yann LeCun^{1 2 3}

Abstract

Self-Supervised Learning (SSL) methods such as VICReg, Barlow Twins or W-MSE avoid collapse of their joint embedding architectures by constraining or regularizing the covariance matrix of their projector’s output. This study highlights important properties of such strategy, which we coin Variance-Covariance regularization (VCR_{eg}). More precisely, we show that *VCR_{eg} combined to a MLP projector enforces pairwise independence between the features of the learned representation*. This result emerges by bridging VCR_{eg} applied on the projector’s output to kernel independence criteria applied on the projector’s input. We empirically validate our findings where (i) we put in evidence which projector’s characteristics favor pairwise independence, (ii) we demonstrate pairwise independence to be beneficial for out-of-domain generalization, (iii) we demonstrate that the scope of VCR_{eg} goes beyond SSL by using it to solve Independent Component Analysis. This provides the first theoretical motivation and explanation of MLP projectors in SSL.

1. Introduction

Self-Supervised Learning (SSL) via joint embedding architectures has risen to learn visual representations outperforming their supervised counterpart. This paradigm enforces similar embeddings for two augmented versions of the same sample, thus allowing an encoder f to learn a representation for a given modality without labels. Importantly, f could solve the learning task by predicting the same embedding for every input, a failure mode known as collapse. To avoid this, various mechanisms have been proposed hence the diversity of SSL methods (e.g., Grill et al. (2020); Caron

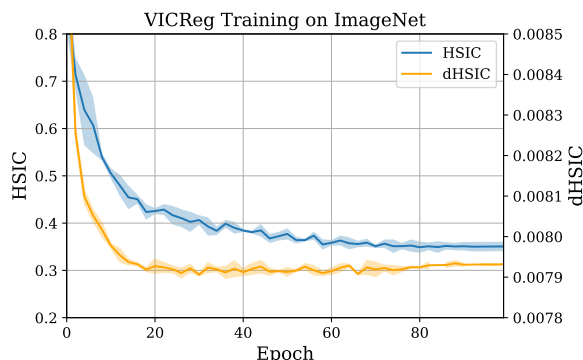


Figure 1. Pairwise independence (HSIc) of the features in the learned representation increases during training while mutual independence (dHSIc) stagnates: VCR_{eg} of the projector implicitly optimizes the former but not the latter. Averaged over three runs.

et al. (2020; 2021); Chen & He (2021)). Most of these are a composition $g \circ f$ of the encoder with a projector neural network g . Only f is retained after training, in opposition to supervised training that never introduces g . The projector was proposed by Chen et al. (2020) and significantly improved the quality of the learned representation in terms of test accuracy on ImageNet and other downstream tasks. Although some works (Appalaraju et al., 2020; Bordes et al., 2022) provide empirical knowledge on the projector, none provide a theoretical analysis of MLP projectors in practical SSL (Jing et al., 2021; Huang et al., 2021; Wang & Isola, 2020; HaoChen et al., 2021; Tian et al., 2020; Wang & Liu, 2021; Cosentino et al., 2022).

This study sheds a new light on the role of the projector via the lens of Variance-Covariance Regularization (VCR_{eg}), a strategy introduced in recent SSL methods (Bardes et al., 2022; Zbontar et al., 2021; Ermolov et al., 2021) to cope with collapse by constraining or regularizing the covariance or cross-correlation of the projector g output to be identity. More precisely, we demonstrate that *VC regularization of the projector’s output enforces pairwise independence between the components of the projector’s input i.e. the encoder’s output*, and connects this property to projector’s characteristics such as width and depth. This provides the first theoretical motivation and explanation of MLP projector in SSL: fully or partially pairwise independent represen-

¹Meta ²Courant Institute, New York University ³Center for Data Science, New York University. Correspondence to: Grégoire Mialon <gmialon@meta.com>.

tations are generally sought for, *e.g.* to disentangle factors of variation (Träuble et al., 2021). In particular, Li et al. (2019) demonstrates that factors in real-world data tend to be pairwise independent. Our experimental analysis suggests that different levels of pairwise independence of the features in the representation emerge from a variety of SSL criteria along with mutual independence. However, as opposed to other frameworks, VCREg allows for theoretical study and explicit control of the learned independence amount. We prove and experimentally validate this property for random projectors, study how it emerges in learned projectors, and demonstrate pairwise independence to be beneficial for out-of-domain generalization. We then ablate the SSL context and lean on our findings to show that VCREg of a SSL projector solves Independent Component Analysis (ICA). Beyond providing a novel theoretical understanding of the projector, we believe that this work also leads to a better understanding of VICReg. The scope of VCREg is not limited to SSL: our experiments on ICA open the way to other applications where some degree of independence is needed.

2. Background

2.1. Measuring Statistical Independence Using Kernel Methods

Measuring the independence between two sets of realizations $\{\mathbf{X}_1^1, \dots, \mathbf{X}_1^N\}, \{\mathbf{X}_2^1, \dots, \mathbf{X}_2^N\}$, $\mathbf{X}_1^i \in \mathbb{R}^M$, $\mathbf{X}_2^i \in \mathbb{R}^M$ is a fundamental task that has a long history in statistics *e.g.* through the Mutual Information (MI) of the two random variables X_1 and X_2 from which those two sets are independently drawn from (Cover, 1999). Those variables are said independent if the realization of one does not affect the probability distribution of the other. Computing the MI in practice is known to be challenging (Goebel et al., 2005), which has led to considerable interest in using alternative criteria *e.g.* based on functions in Reproducing Kernel Hilbert Spaces (RKHS) (Bach & Jordan, 2002), a special case of what is known as functional covariance or correlation (Rényi, 1959). It consists in computing those statistics after nonlinear transformation (Leurgans et al., 1993) as in

$$\sup_{f_1 \in \mathcal{F}_1, f_2 \in \mathcal{F}_2} \text{Corr}\langle f_1(X_1), f_2(X_2) \rangle, \quad (1)$$

where f_1, f_2 are constrained to lie within some designed functional space, and the Cov can be used instead of the Corr. If Equation (1) is small enough, then X_1 and X_2 are independent in regard to the functional spaces $\mathcal{F}_1, \mathcal{F}_2$. For example, if \mathcal{F}_1 and \mathcal{F}_2 are unit balls in their respective vector spaces, then Equation (1) is just the norm of the usual correlation/covariance operator (Mourier, 1953) which would be enough for independence under joint Gaussian distributions (Melnick & Tenenbein, 1982).

HSIC and pairwise independence. More recently, Gretton et al. (2005a) introduced a pairwise independence criterion known as the Hilbert-Schmidt Independence Criterion (HSIC) between the two random variables X_1 and X_2 which can be estimated given empirical samples \mathbf{X}_1 and $\mathbf{X}_2 \in \mathbb{R}^{N \times M}$ via

$$\text{HSIC}(\mathbf{X}_1, \mathbf{X}_2) := \frac{1}{(N-1)^2} \text{Tr}(\mathbf{K}_1 \mathbf{H} \mathbf{K}_2 \mathbf{H}), \quad (2)$$

with \mathbf{H} the centering matrix $\mathbf{I} - \mathbf{1}\mathbf{1}^T \frac{1}{N}$, $(\mathbf{K}_1)_{i,j} = k_1(\mathbf{X}_1^i, \mathbf{X}_1^j)$ and $(\mathbf{K}_2)_{i,j} = k_2(\mathbf{X}_2^i, \mathbf{X}_2^j)$ the two kernel matrices of \mathbf{X}_1 and \mathbf{X}_2 respectively, and k_1, k_2 of $\mathcal{F}_1, \mathcal{F}_2$ universal kernels such as the Gaussian kernel (see Steinwart (2001); Micchelli et al. (2006) for other examples). Crucially, since

$$\text{HSIC}(X_1, X_2) \geq \sup_{f_1 \in \mathcal{F}_1, f_2 \in \mathcal{F}_2} \text{Cov}\langle f_1(X_1), f_2(X_2) \rangle, \quad (3)$$

HSIC can be used to test for (pairwise) independence as formalized below.

Theorem 2.1 (Thm. 4 from (Gretton et al., 2005a)). *HSIC(X_1, X_2) = 0 if and only if X_1 and X_2 are independent.*

(Gretton et al., 2005a) also provide a statistical test for pairwise independence based on HSIC. Further quantities such as upper bounds on the MI can be found in a similar way, *e.g.* see Thm. 16 in (Gretton et al., 2005b). In our experiments, we rely on HSIC under the Gaussian kernel scaled by the median of the distribution of pairwise euclidean distances between samples. To compare HSIC across different models, we further normalize following Kornblith et al. (2019).

dHSIC and mutual independence. Mutual independence of a set of D M -dimensional random variables X_1, \dots, X_D is a stronger property than independence between all pairs of random variables in the set. To evaluate it, Pfister et al. (2018) introduce dHSIC, a multivariate extension of HSIC. In short, $\text{dHSIC}(X_1, \dots, X_D)$ measures the distance between mean embeddings μ under a RKHS \mathcal{F} (Smola et al., 2007) of the product of distributions and the joint distribution

$$\|\mu(\mathbb{P}^{X_1} \otimes \dots \otimes \mathbb{P}^{X_D}) - \mu(\mathbb{P}^{X_1, \dots, X_D})\|_{\mathcal{F}}. \quad (4)$$

Similarly to HSIC, Pfister et al. (2018) establish the equivalence between $\text{dHSIC} = 0$ and mutual independence along with a statistical test. We provide an estimator of dHSIC given empirical samples $\mathbf{X}_1, \dots, \mathbf{X}_D$ of the above random variables in $\mathbb{R}^{N \times M}$ each as well as implementations of HSIC and dHSIC in Appendix D.

Complexities. In what follows, we consider the D features of a batch of representations $\mathbf{X} \in \mathbb{R}^{N \times D}$ as D scalar

random variables ($M = 1$) with N samples each. The subsequent complexities of HSIC for one pair of features and dHSIC are $\mathcal{O}(N^2)$ and $\mathcal{O}(DN^2)$ respectively. Testing pairwise independence between all variables in a D -set with HSIC is $\mathcal{O}(D^2N^2)$ while dHSIC requires $N \geq 2D$ (Pfister et al., 2018). Since competitive visual representations typically have $D = 2048$, we resort to surrogates to estimate independence of the representations in practice. These surrogates are detailed in Section 5.

2.2. Variance-Covariance Regularization in Self-Supervised Learning

SSL with joint embeddings learns visual representations by producing two different augmented views of an input batch of images $\mathcal{S} \in \mathbb{R}^{N \times W \times H}$, denoted by $\mathcal{S}_{\text{left}}$ and $\mathcal{S}_{\text{right}}$. Each view is fed to an encoder f , typically a ResNet50 (He et al., 2016), producing representations \mathbf{X}_{left} and $\mathbf{X}_{\text{right}} \in \mathbb{R}^{N \times D}$ which are passed through a projector g to output embeddings \mathbf{Z}_{left} and $\mathbf{Z}_{\text{right}} \in \mathbb{R}^{N \times P}$. Finally, an invariance term encouraging \mathbf{Z}_{left} and $\mathbf{Z}_{\text{right}}$ to be similar is applied. While most SSL methods require architectural or training strategies to avoid collapse (Grill et al., 2020; He et al., 2021), Bardes et al. (2022) and Zbontar et al. (2021) only require to modify the loss. After training, only f is retained to be used in downstream tasks. We will denote the $(2N, P)$ matrix $\mathbf{Z}_{\text{total}} \triangleq [\mathbf{Z}_{\text{left}}^T, \mathbf{Z}_{\text{right}}^T]^T$. More background on self-supervised learning for images in theory and in practice can be found in Appendix A. In particular, we detail the crucial role of the projector in many SSL frameworks.

VICReg. In Bardes et al. (2022), an anti-collapse term \mathcal{L}_{VC} , which we coin VC regularization (VCReg), is added to an invariance loss to form \mathcal{L}_{VIC} :

$$\mathcal{L}_{\text{VC}} = \sum_{k=1}^P \max \left(0, 1 - \sqrt{\text{Cov}(\mathbf{Z}_{\text{total}})_{k,k}} \right) + \alpha \sum_{j=1, j \neq k}^P \text{Cov}(\mathbf{Z}_{\text{total}})_{k,j}^2, \quad (5)$$

$$\mathcal{L}_{\text{VIC}} = \frac{1}{N} \sum_{n=1}^N \|(\mathbf{Z}_{\text{left}})_{n,\cdot} - (\mathbf{Z}_{\text{right}})_{n,\cdot}\|_2^2 + \mathcal{L}_{\text{VC}}, \quad (6)$$

The leftmost term in \mathcal{L}_{VC} corresponds to regularizing the variance of each feature in $\mathbf{Z}_{\text{total}}$ to be at least unit, while the second term seeks to minimize the covariance between each pair of features in $\mathbf{Z}_{\text{total}}$. Note that \mathcal{L}_{VC} applies to each view separately. In Bardes et al. (2022), the weight of each term in \mathcal{L}_{VIC} can be tuned. Since the authors find that best results are obtained with equal weights for the invariance and the variance terms, we only vary α . Note that Bardes et al. (2022); Zbontar et al. (2021) observe that wider projectors further improve the representation learned

by the encoder f , yet neither further study this intriguing phenomenon. Although this work focuses on VCReg as formulated in VICReg, we provide background on Barlow Twins and W-MSE in the Appendix A, while next section establishes the similarity between VICReg, Barlow Twins and W-MSE as VCReg optimizers.

3. VC Regularization of SSL Projector’s Output Enforces Pairwise Independent Features at the Encoder’s Output

In this section, we demonstrate that for random Multi-Layer Perceptrons (MLPs) projectors, minimizing VC of the projector’s output amounts to minimizing HSIC—a measure of pairwise dependence (see Section 2.1)—between all pairs of features in the learned representation, *i.e.* the projector’s input. The randomness assumption has already been used to model weight evolution during training (Franchi et al., 2020; Blundell et al., 2015). We then justify how this reasoning extends to learned projectors. Our claims are experimentally verified in Section 5.

Notations. In our setting, $\mathbf{X} \in \mathbb{R}^{N \times D}$ is the D dimensional output of the encoder f for a batch of size N . \mathbf{X} is then fed to the projector g to form embeddings $\mathbf{Z} = g(\mathbf{X}) = [g\mathbf{X}_1, \dots, g\mathbf{X}_P] \in \mathbb{R}^{N \times P}$ on which SSL criteria are generally applied. Note that \mathbf{Z} would be \mathbf{Z}_{left} or $\mathbf{Z}_{\text{right}}$ in the previous subsection. The acronym MLP refers to projectors typically used in SSL, a neural network with three layers of same width, unless stated otherwise.

Our proof strategy consists in proving that VCReg of each MLP layer (Linear + Batch Normalization (BN) + ReLU) output enforces pairwise independence of its input, before composing these results. We first study nonlinear elementwise projectors $g : \mathbb{R} \mapsto \mathbb{R}^L$, which belong to the wider class of DeepSets (Zaheer et al., 2017), and of which BN followed by ReLU can be seen as an instance. We denote the mapping of such projectors as $\mathbf{Z} = g(\mathbf{X}) = [g(\mathbf{X}_{:,1}), \dots, g(\mathbf{X}_{:,P})]$.

Lemma 3.1 (Nonlinear elementwise projectors minimize HSIC of their input). *Let $g : \mathbb{R} \mapsto \mathbb{R}^L$ be a nonlinear elementwise projector; then, minimizing the covariance of \mathbf{Z} with respect to the encoder f amounts to minimizing HSIC on all feature pairs in \mathbf{X} under the kernels $\mathbf{K}_i = g(\mathbf{X}_{:,i})g(\mathbf{X}_{:,i})^T$.*

Proof. Let us consider the N values of the i^{th} data feature $(\mathbf{X}_{:,i})$ as realizations of a random variable. Recalling Equation (2), independence of two random variables can be estimated via HSIC. Considering the arbitrarily complicated network g and $\mathbf{Z} = [g(\mathbf{X}_{:,1}), \dots, g(\mathbf{X}_{:,D})] \in \mathbb{R}^{N \times DL}$, we

have:

$$\begin{aligned}
 \text{HSIC}(\mathbf{X}_{:,i}, \mathbf{X}_{:,j}) &= \frac{\text{Tr}(g(\mathbf{X}_{:,i})g(\mathbf{X}_{:,i})^T \mathbf{H} g(\mathbf{X}_{:,j})g(\mathbf{X}_{:,j})^T \mathbf{H})}{(N-1)^2} \\
 &= \frac{1}{(N-1)^2} \|g(\mathbf{X}_{:,i})^T \mathbf{H} g(\mathbf{X}_{:,j})\|_F^2 \\
 &= \|\text{Cov}(g(\mathbf{X}_{:,i}), g(\mathbf{X}_{:,j}))\|_F^2 \\
 &= \left\| \text{Cov}(\mathbf{Z})_{1+iL:1+(i+1)L, 1+jL:1+(j+1)L} \right\|_F^2
 \end{aligned}$$

Hence,

$$\sum_{i \neq j} \text{HSIC}(\mathbf{X}_{:,i}, \mathbf{X}_{:,j}) = \left\| \text{Cov}(\mathbf{Z}) \odot ((1 - \mathbf{I}_D) \otimes \mathbf{1}_L \mathbf{1}_L^T) \right\|_F^2,$$

and, in the case $L = 1$ we have $\mathbf{1}_L \mathbf{1}_L^T = \mathbf{1}$ leading to $\sum_{i \neq j} \text{HSIC}(\mathbf{X}_{:,i}, \mathbf{X}_{:,j}) = \sum_{i \neq j} \text{Cov}(\mathbf{Z})_{i,j}^2$, concluding the proof. \square

To rigorously obtain independence, the \mathbf{K}_i 's must be universal kernels. In practice, Batch Normalization in the projector can be considered random as it uses the batch statistic. Combining this operation with a ReLU, we obtain random elementwise nonlinearities approaching random features (Rahimi & Recht, 2007) of a universal kernel (Sun et al., 2018). Increasing L improves the approximation of such kernel (Chen & Phillips, 2017) i.e. the larger L , the better approximation of HSIC the covariance term in VICReg is.

Remark 3.2 (Necessity of variance regularization). Although the variance regularization term does not explicitly appear when minimizing HSIC on all pairs, it is necessary when optimizing \mathbf{X} to prevent the degenerate solution of \mathbf{X} being a constant, a common collapse mode of SSL.

Lemma 3.3 (Random linear projectors minimize HSIC of their input). *Let g be a random linear projector with weights \mathbf{W} , and \mathbf{X} has same variance for each column. Then, for large projectors, minimizing the covariance of $\mathbf{Z} = g(\mathbf{X}) = \mathbf{X}\mathbf{W}$ with respect to the encoder f amounts to minimizing HSIC with a linear kernel for each pair of features in \mathbf{X} . (Proof in Appendix B.1.)*

Since the corresponding kernel in Lemma 3.3 is linear, only decorrelation can be achieved for such projector's input. This however differs from PCA, as we optimize over \mathbf{X} and not g 's parameters (\mathbf{W}). Proving Lemma 3.3 requires a projector with orthogonal weights, i.e. $\mathbf{W}^T \mathbf{W} = \mathbf{I}$, which gets more and more accurate with random weights $\mathcal{U}(-1/\sqrt{D}, 1/\sqrt{D})$ as P (the output dimension of g) increases. This follows since the central limit theorem states that the dot-product between two P -dimensional weight vectors tends to 0 with rate $\mathcal{O}(1/\sqrt{P})$. Weight initialization in neural nets roughly follows $\mathcal{U}(-1/\sqrt{D}, 1/\sqrt{D})$, which will be used to instantiate random projectors.

Theorem 3.4 (MLP projectors with random weights enforce pairwise independence.). *Let us consider a MLP composed of alternating random linear layers and elementwise nonlinearities. Then, for large projectors, minimizing the variance and covariance of the output \mathbf{Z} enforces pairwise independence between all pairs of features in the input \mathbf{X} .*

Proof. Let us consider the last block of such MLP, i.e. a fully-connected linear layer followed by an elementwise nonlinearity. According to Lemma 3.1, applying VCReg to the MLP, i.e. at the output of the nonlinearity will enforce pairwise independence under corresponding kernel for the input of the nonlinearity, which is also the output of the last linear layer. If the latter is wide enough so that it can be considered orthogonal, Theorem 11 in (Comon, 1994) ensures that pairwise independence is preserved for the input of the layer. We can then recursively extend the result backward to the whole MLP. If the last MLP layer is a fully-connected linear, then Lemma 3.3 applies and we go back to the preceding elementwise nonlinearity. \square

Figure 7 in Appendix C.2 shows that each hidden layer in the random MLP is recursively and implicitly VC-regularized from VCReg being applied only at the projector's output. Following Theorem 3.4, we expect wider projectors to better enforce pairwise independence while adding layers or learning the projector is not necessary; see Section 5 for empirical validation.

Extension to BarlowTwins and W-MSE, and generality of VCReg.

Our results focus on VCReg as formulated in VICReg but can in fact be extended to methods that constrain the covariance of \mathbf{Z} explicitly, namely BarlowTwins and W-MSE (Balestriero & LeCun, 2022). Indeed, the objective in W-MSE (Equations 3-4 in Ermolov et al. (2021)) is VICReg with explicit constraint on the variance and covariance. Increasing the variance and covariance hyper-parameters in VICReg produces W-MSE hence our results extend seamlessly. The objective from Equation (7) in BarlowTwins is also similar to VICReg. The derivation, deferred to Appendix B.2, shows that minimizing the constrained form of BarlowTwins objective from Equation (7) is equivalent to minimizing VICReg's invariance term whilst explicitly constraining the variance covariance terms as in W-MSE; hence our results also hold for BarlowTwins; see Section 5 for empirical validation. In particular we will see that as BarlowTwins explicitly enforces minimum VCReg, it better optimizes HSIC compared to VICReg with standard hyper-parameters. Finally, as opposed to BarlowTwins loss and most SSL methods, VCReg can be used and be beneficial within single branch architectures. We provide such use case in Section 5.

Learned projectors. In state-of-the-art SSL representations, the projector is learned, which is not rigorously covered by Theorem 3.4. Complementing the study of (Bordes et al., 2022), we argue that learning the projector is only crucial to satisfy the invariance criterion since random projectors are sufficient to obtain pairwise independent features, as demonstrated in Section 5. In fact, our experiments show that (i) using VICReg, keeping the projector random yield representations with low HSIC, (ii) using VICReg, learning the projector to optimize VCRreg more strongly than the invariance term reduces performances, and (iii) using VCRreg without an invariance term, learning the projector (e.g. in the later studied ICA setting) creates a degenerate representation that does not enforce pairwise independence. We thus conjecture that learning the projector’s parameters to mainly minimize VICReg’s invariance term leaves the parameters close enough to their random initialization (Jacot et al., 2018) to maintain an accurate estimate of HSIC. In fact, we will see that the wider the projector, the less far away from initialization the parameters have to move, and the better optimized HSIC. Importantly, to better mimic the behavior of a learned projector, we will also conduct experiments where the random projector is resampled at each optimization step.

4. Related Work

Feature decorrelation, or whitening, ensures that correlation between each pair of different features in a batch of feature vectors is zero, and that each feature has unit variance. It was originally used as a data pre-processing technique, see e.g. (Hyvärinen & Oja, 2000), before being extended to deep networks (Cogswell et al., 2015) as a regularizer. In the context of SSL, Hua et al. (2021); Ermolov et al. (2021) find that feature decorrelation helps solving the collapse issue. The former avoids collapse via appropriate Batch Normalization and its decorrelating variant (Huang et al., 2018) in the projector. This variant of Batch Normalization can be seen as the hard constraint counterpart of BarlowTwins. Practically, whitening can be implemented by learning a fully-connected layer (Husain & Bober, 2019) recovering Principal Component Analysis; as mentioned earlier (Section 3), this differs from VCRreg which keeps the layer’s parameters random and optimizes its input.

Independence criterion for learning features. Enforcing mutual independence to learn a representation has been proposed for example by Schmidhuber (1992). More recently, and in the context of supervised learning, Chen et al. (2019) demonstrated improved training of ResNets by reducing the pairwise dependence in the features at each layer via a combination of Dropout and Batch Normalization. By opposition, VCRreg is applied to the projector’s output and common SSL projectors do not rely on Dropout; we also

show that Batch Normalization is not necessary to reduce pairwise dependence.

HSIC in supervised and self-supervised learning. HSIC-based losses have been employed in supervised learning e.g. see Mooij et al. (2009); Greenfeld & Shalit (2020) to ensure independence between the residual errors and the labels of a task at hand. Kornblith et al. (2019) measure similarity between two neural representations via HSIC. In SSL, Tsai et al. (2021) showed that a modified version of BarlowTwins loss maximizes HSIC under a linear kernel between the embeddings of two augmented versions of the same sample. In a similar fashion, Li et al. (2021) proposed a SSL framework based on maximizing the dependence between the embeddings of transformations of an image and the image identity via HSIC. Both works differ from ours, which connects VCRreg to the minimization of HSIC between pairs of features in the representation.

5. Experiments

We first put in evidence pairwise independence properties emerging in learned visual representations, before validating our theoretical findings from Section 3. Then, we demonstrate low HSIC to be beneficial for in-domain and out-of-domain generalization. Finally, we ablate the SSL context and demonstrate that the composition of a SSL-like random projector with VCRreg induces enough independence to perform ICA. Importantly, none of the experiments with VCRreg use Dropout, and Batch Normalization is not used when the projector is random. Hence, pairwise independence cannot be attributed to those two techniques as opposed to Chen et al. (2019); Hua et al. (2021).

5.1. Pairwise independence emerges in most visual representations

Setup. In these experiments, we track two metrics for statistical independence of the components in the learned representation during ResNet50 training on ImageNet with popular SSL frameworks, as well as a supervised baseline. The first metric, HSIC (Gretton et al., 2005a), tracks pairwise independence. The second metric, dHSIC (Pfister et al., 2018), tracks mutual independence. As explained in Section 2.1, neither HSIC nor dHSIC scale to the full representation (2048 components). Therefore, we instead rely on proxies: for pairwise independence, we compute and average Normalized HSIC (Kornblith et al., 2019) on all pairs of the first 10 components of the representation. For mutual independence, we sample sets of 10 components for which we display dHSIC. We compute these statistics on the same batch of 1000 samples (one per class) from the ImageNet validation set unless stated otherwise. A decrease of these metrics throughout the training would suggest de-

Table 1. Pairwise dependence (HSIC), pairwise independence testing, and test accuracy for SSL or supervised representations averaged on multiple subsets of features, with internal variance. VCReg methods, including SimCLR (Garrido et al., 2022), further improve HSIC.

Method (100 epochs)	Normalized HSIC ↓	% of independent pairs ↑	ImageNet Top1 ↑
BarlowTwins (Zbontar et al., 2021)	0.006 ± 0.004	38 ± 2	67.8
SimCLR (Chen et al., 2020)	0.008 ± 0.008	36 ± 1	67.7
VICReg (Bardes et al., 2022)	0.009 ± 0.005	34 ± 2	68.1
DINO (Caron et al., 2021)	0.01 ± 0.01	35 ± 3	70.4
Supervised (Wightman et al., 2021)	0.010 ± 0.008	33 ± 3	78.1

creasing dependence among the representations. Although statistical tests are available for both metrics, we track bare HSIC and dHSIC as they are continuous. However, we perform HSIC tests in this first series of experiments so that the bare values can be linked to portions of independent pairs of components in the representation. See Appendix E for our detailed setup.

Results. Figure 1 suggests that VICReg implicitly optimizes pairwise independence of the features in the representation throughout the training (HSIC, left), but not mutual independence (dHSIC, right). We will therefore not study dHSIC in subsections 5.2 and 5.3, while an ablation in subsection 5.4 further confirm that VCReg cannot optimize dHSIC. Table 1 shows that VCReg frameworks (VICReg, Barlow Twins) and related (SimCLR¹) achieve lower HSIC than DINO and Supervised, and Barlow Twins better enforces low HSIC since its covariance matrix is constrained, as expected from Section 3. Precise values along with HSIC independence tests at level $\alpha = 0.5$ and corresponding test accuracies can be found in Table 1. Lower HSIC values do not necessarily entail more successful tests: it is possible to allocate low HSIC to sufficiently many pairs while having an overall larger HSIC. For example, Supervised has less independent pairs in spite of an overall smaller HSIC than DINO. Table 1 also suggests that pairwise independence is not perfectly predictive of test accuracy. Although it seems to be a desirable property, it is not sufficient to yield a good representation: for example, DINO achieves better test accuracy than BarlowTwins in spite of higher HSIC. Section 5.3 will however show and discuss how HSIC is correlated with in domain and out of domain downstream accuracy.

5.2. Projector characteristics fostering or hurting pairwise independence

Setup. These experiments validate the results from Section 3 by illustrating which projector characteristics help or hurt HSIC optimization when learning visual representations. The setup is the same as above except that dHSIC is not measured. However, the projector can be random

¹ Garrido et al. (2022) demonstrate that up to implementation details, VICReg and SimCLR optimize the same objective and can in fact achieve the same performance with careful hyperparameter tuning.

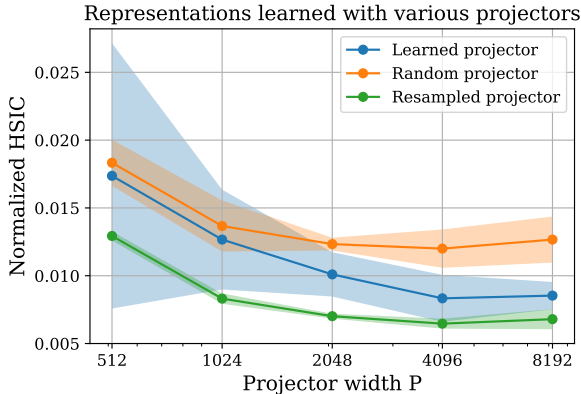


Figure 2. Normalized HSIC (computed on ImageNet validation) for various representations learned with different projectors width and setup: learned, random, random and resampled at each optimization step (3 runs each). Wider projectors and resampling both yield more pairwise independence in the learned representation.

with resampling at each optimization step or without, as in Theorem 3.4, or learned as in Section 5.1. We apply an invariance loss along with VCReg on the output of the projector and scale the covariance coefficient with its width P for fair comparison since the covariance term in VCReg grows quadratically with the projector output dimension (see Equation (5)). See Appendix E for our detailed setup.

Results. Figure 2 supports the theory from Section 3: low HSIC can be achieved by random projectors. Hence, learning the projector is not necessary to obtain pairwise independence. As predicted in theory, for all three settings, HSIC is better optimized for wider projectors. HSIC can be influenced by other factors of variations: as conjectured in Section 3, for random projectors, increasing depth hurts HSIC, see Figure 8 in Appendix C.2. Increasing the covariance coefficient in VCReg also improves HSIC, albeit slightly at the expense of downstream accuracy, see Table 4 in Appendix C.2. We observe that (i) random resampled projectors from Section 3 learn representations with better pairwise independence properties than learned projectors –we will heavily use this property in Section 5.4–, and (ii) random projectors do worse. (i) can be explained by the fact that learning the projector to optimize VCReg is detrimental to HSIC since it could achieve trivial solutions such as $Z = g(X) = (X_1, 0, \dots, 0)$: the presence of the invariance

term explains why a learned projector does not collapse on such solutions. (ii) can be explained as follow: since the projector weights are fixed, the encoder only learns to decorrelate a limited set of nonlinear functions as opposed to the random resampled or learned projectors, whose weights move throughout the training. Although random resampled projectors achieve lower HSIC, most of them are not as competitive as learned projectors in terms of in domain test accuracy of the learned representation, see Table 2. This is not surprising, as there is no reason for the best $D = 2048$ representations for ImageNet to have all their features pairwise independent. In fact, this suggests that optimizing too much HSIC can be detrimental for the quality of the representation: a possible explanation is that it is not possible to extract all the relevant information from the training set with respect to classification while preserving total pairwise independence in the representation. This complements the view of (Appalaraju et al., 2020; Bordes et al., 2022), which argue that the projector requires some learning capacity to filter out information that is irrelevant to fulfill the invariance loss. Finally, Figure 8 in Appendix C shows that adding layers to random projectors is detrimental to HSIC: implicit VCRreg of the activations, an assumption of Theorem 3.4, will be more and more loosely enforced. These experiments suggest that the projector capacity should rather be increased via width than via depth: adding layers can be detrimental to HSIC as seen above but also to test accuracy (Appalaraju et al., 2020; Chen et al., 2021).

Table 2. Normalized HSIC (divided by 1e3 for readability) and Top1 accuracy on ImageNet (both computed on validation) for representations learned with different projector types ($P = 8192$).

Projector type	Random	Learned	Resampled
Norm. HSIC (\downarrow)	13 ± 2	9 ± 1	6.8 ± 0.1
Top1 ImageNet (\uparrow)	54.1 ± 0.1	68.12 ± 0.01	52.5 ± 0.2

5.3. HSIC is correlated to in-domain and out-of-domain downstream accuracy

In this experiment, we plot the Normalized HSIC and Relative Top1 accuracy on various datasets for the representations trained in this work, *i.e.*, for various projector configurations, see Figure 3. Overall, HSIC is correlated to in-domain and out-of-domain downstream accuracy. As expected from Table 2, an elbow appears around Normalized HSIC = 0.008: below this threshold, the representation gains pairwise independence at the expense of its information content, a form of collapse. Crucially, HSIC does not require labels to be computed hence could be used for model selection in SSL.

5.4. Ablation: Independent Component Analysis (ICA) with VCRreg

To demonstrate that our findings hold outside of SSL, we show that VCRreg of a SSL-like projector’s output induces

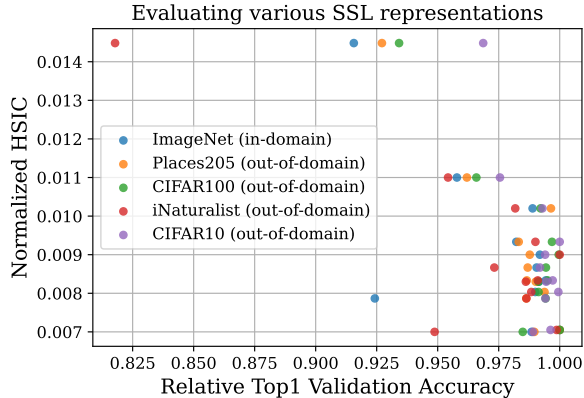


Figure 3. Normalized HSIC (computed on ImageNet validation) of representations correlates with downstream accuracy both in domain and out of domain. To each HSIC level corresponds a representation. For each dataset, the accuracies were rescaled with respect to their maximum for better readability.

enough pairwise independence to solve linear ICA, *i.e.* recovering independent sources $S \in \mathbb{R}^{N \times D}$ from a mixture $Y = SA \in \mathbb{R}^{N \times D}$. See Appendix A for an introduction to ICA.

VC regularized random projectors solve linear ICA, learned projector don’t. In this setting, finding M enforcing pairwise independence in the components of YM is generally sufficient to recover S ((Comon, 1994), Theorem 11). VCRreg of a random projector’s output should therefore be able to recover S . Our model can be seen on Figure 4: whitened batches of mixtures Y are fed to an encoder f . Here, f is a linear transformation M described above. The output $X = f(Y)$ is then fed to a projector g , and VCRreg is applied to the output $Z = g(X)$ covariance matrix. As in Experiments 5.2, the projector is randomly resampled at each gradient step to get lowest possible HSIC. This setting corresponds to one branch of a VICReg network (i) with a linear projection M encoder instead of a neural network, (ii) with a random projector, and (iii) without invariance criterion. We perform ICA on two datasets, a synthetic one (Brakel & Bengio, 2017) with 6 sources among which 2 are noise, and a real audio dataset (Kabal, 2002) with 3 sources among which one is noise, also used in (Brakel & Bengio, 2017). The evaluation metric is the maximum correlation between true and reconstructed sources. This metric is not available without ground truth hence we select the model with lowest dHSIC for X , which can be exactly evaluated since the number of sources is small.

Our model recovers the sources, and is even competitive with methods specifically designed for linear ICA such as Fast ICA (Hyvärinen & Oja, 2000) or Anica (Brakel & Bengio, 2017), see Table 3. Both increasing the width of the projector and resampling it at each step (especially for smaller projectors) improve the reconstruction as can

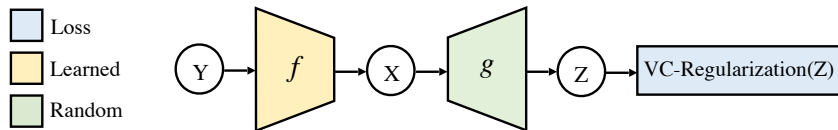


Figure 4. Linear ICA model expressed from VCRg of the projector’s output.

Table 3. Maximum correlation between true and reconstructed sources (the higher the better \uparrow). The projector performs competitive reconstruction in the linear setting (left), where pairwise independence is sufficient, but not in PNL (right) where it is not.

Linear mixture			Post Non Linear mixture		
Method	Synthetic data	Audio data	Method	Synthetic data	Audio data
Whitening	0.8074	0.9876	Whitening	0.7981	0.9046
FastICA	0.9998	1.0	FastICA	0.8311	0.8989
Anica	$0.9987 \pm 6.5e-4$	$0.9996 \pm 4.9e-4$	Anica	$0.9794 \pm 53e-4$	$0.9929 \pm 18e-4$
VCRg	$0.9986 \pm 8.2e-4$	$0.9936 \pm 64e-4$	VCRg	$0.8465 \pm 142e-4$	$0.8706 \pm 376e-4$

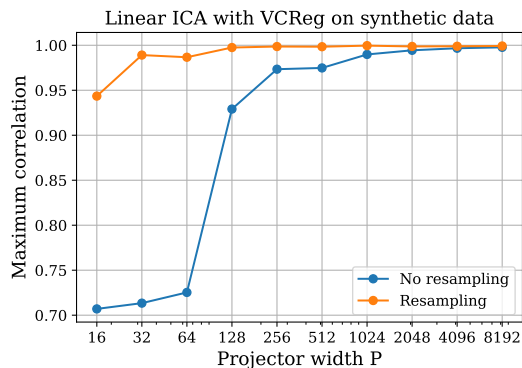


Figure 5. Resampling and increased width of the projector g both improve the quality of the source reconstruction measured by the maximum correlation between true and reconstructed sources (\uparrow).

be seen in Figure 5. This is in line with our findings in Section 3 and Experiment 5.2. ICA experiments done with a learned projector fail to recover independent sources: this further demonstrates that learning the projector to optimize VCRg is counter-productive, and that in the context of SSL, learning the projector is rather useful for satisfying the invariance criterion, which is absent in the ICA experiments. VCRg is rather optimized by the encoder f .

VC regularized projectors do not solve nonlinear ICA.

Figure 1 suggests that mutual independence is optimized during training although not properly: one could ask whether VCRg also enforces it enough to solve nonlinear ICA. To test this hypothesis, we apply VCRg to a particular case of nonlinear ICA which allows identifiability but does not have equivalence between pairwise and mutual independence: the post-nonlinear mixture (PNL) (Taleb & Jutten, 1999). In PNL, the sources are linearly mixed before being fed to elementwise nonlinear functions. For these

experiments, and following (Brakel & Bengio, 2017), our encoder is a MLP. During our first experiments, we observed an informational collapse of the encoder, which produces seemingly mutually independent variables with very poor reconstruction of the sources. To alleviate this issue, we add a decoder taking X as input and reconstructing Y . Figure 9 in Appendix E shows our modified setup. We compare VCRg to FastICA and Anica. Although FastICA is not meant to solve the nonlinear case, it remains an interesting baseline. Table 3 shows that our model fails to recover the sources, as it does only slightly better than FastICA in the synthetic case. Hence, although mutual independence increases during training, VCRg does not optimize it enough to solve nonlinear ICA. We propose a simple explanation for this limitation. Indeed, each feature in Z is a nonlinear function of all features in X . Hence, it is not possible to completely decorrelate two components of Z as they both contain the same set of features. It is still possible to improve mutual independence to some extent since, in practice, only parts of the inputs are considered at once by nonlinear mappings such as neural networks (Erhan et al., 2009; Adebayo et al., 2018).

6. Conclusion

This work provides the first theoretical explanation of SSL projectors by demonstrating they enforce pairwise independence in the learned representation. This quantity is correlated to in-domain and out-of-domain downstream accuracy and could be further exploited for model selection without labels. The classical evaluation of SSL being linear probing, further work could also explore whether pairwise independence is connected to linear separability of the features. Finally, this work focuses on random weights with uniform distribution yet opens the way to weight distributions that are closer to training parameters in practice which, for example, have been characterized for over-parameterized networks (Jacot et al., 2018).

References

- Adebayo, J., Gilmer, J., Muelly, M., Goodfellow, I., Hardt, M., and Kim, B. Sanity checks for saliency maps. *Advances in Neural Information Processing Systems (NeurIPS)*, 2018.
- Appalaraju, S., Zhu, Y., Xie, Y., and Fehérvári, I. Towards good practices in self-supervised representation learning. *arXiv preprint arXiv:2012.00868*, 2020.
- Bach, F. R. and Jordan, M. I. Kernel independent component analysis. *Journal of Machine Learning Research (JMLR)*, 2002.
- Balestriero, R. and LeCun, Y. Contrastive and non-contrastive self-supervised learning recover global and local spectral embedding methods. *arXiv preprint arXiv:2205.11508*, 2022.
- Bardes, A., Ponce, J., and LeCun, Y. Vicreg: Variance-invariance-covariance regularization for self-supervised learning. *International Conference on Learning Representations (ICLR)*, 2022.
- Blundell, C., Cornebise, J., Kavukcuoglu, K., and Wierstra, D. Weight uncertainty in neural networks. In *International Conference on Machine Learning (ICML)*, 2015.
- Bordes, F., Balestriero, R., Garrido, Q., Bardes, A., and Vincent, P. Guillotine regularization: Improving deep networks generalization by removing their head. *arXiv preprint arXiv:2206.13378*, 2022.
- Brakel, P. and Bengio, Y. Learning independent features with adversarial nets for non-linear ica. *arXiv preprint arXiv:1710.05050*, 2017.
- Caron, M., Misra, I., Mairal, J., Goyal, P., Bojanowski, P., and Joulin, A. Unsupervised learning of visual features by contrasting cluster assignments. *Advances in Neural Information Processing Systems (NeurIPS)*, 2020.
- Caron, M., Touvron, H., Misra, I., Jégou, H., Mairal, J., Bojanowski, P., and Joulin, A. Emerging properties in self-supervised vision transformers. In *Proceedings of the IEEE/CVF International Conference on Computer Vision*, pp. 9650–9660, 2021.
- Chen, D. and Phillips, J. M. Relative error embeddings of the gaussian kernel distance. In *International Conference on Algorithmic Learning Theory*, pp. 560–576. PMLR, 2017.
- Chen, G., Chen, P., Shi, Y., Hsieh, C.-Y., Liao, B., and Zhang, S. Rethinking the usage of batch normalization and dropout in the training of deep neural networks. *arXiv preprint arXiv:1905.05928*, 2019.
- Chen, T., Kornblith, S., Norouzi, M., and Hinton, G. A simple framework for contrastive learning of visual representations. In *International Conference on Machine Learning (ICML)*, 2020.
- Chen, T., Luo, C., and Li, L. Intriguing properties of contrastive losses. *Advances in Neural Information Processing Systems (NeurIPS)*, 2021.
- Chen, X. and He, K. Exploring simple siamese representation learning. In *Proceedings of the IEEE/CVF Conference on Computer Vision and Pattern Recognition*, pp. 15750–15758, 2021.
- Cogswell, M., Ahmed, F., Girshick, R., Zitnick, L., and Batra, D. Reducing overfitting in deep networks by decorrelating representations. *arXiv preprint arXiv:1511.06068*, 2015.
- Comon, P. Independent component analysis, a new concept? *Signal processing*, 36(3):287–314, 1994.
- Cosentino, R., Sengupta, A., Avestimehr, S., Soltanolkotabi, M., Ortega, A., Willke, T., and Tepper, M. Toward a geometrical understanding of self-supervised contrastive learning. *arXiv preprint arXiv:2205.06926*, 2022.
- Cover, T. M. *Elements of information theory*. John Wiley & Sons, 1999.
- Dosovitskiy, A., Beyer, L., Kolesnikov, A., Weissenborn, D., Zhai, X., Unterthiner, T., Dehghani, M., Minderer, M., Heigold, G., Gelly, S., et al. An image is worth 16x16 words: Transformers for image recognition at scale. *International Conference on Learning Representations (ICLR)*, 2020.
- Erhan, D., Bengio, Y., Courville, A., and Vincent, P. Visualizing higher-layer features of a deep network. *University of Montreal*, 1341(3):1, 2009.
- Ermolov, A., Siarohin, A., Sangineto, E., and Sebe, N. Whitening for self-supervised representation learning. In *International Conference on Machine Learning (ICML)*, 2021.
- Franchi, G., Bursuc, A., Aldea, E., Dubuisson, S., and Bloch, I. Tradi: Tracking deep neural network weight distributions for uncertainty estimation. In *Proceedings of the European Conference on Computer Vision (ECCV)*, 2020.
- Garrido, Q., Chen, Y., Bardes, A., Najman, L., and LeCun, Y. On the duality between contrastive and non-contrastive self-supervised learning. *arXiv preprint arXiv:2206.02574*, 2022.
- Goebel, B., Dawy, Z., Hagenauer, J., and Mueller, J. C. An approximation to the distribution of finite sample size

- mutual information estimates. In *IEEE International Conference on Communications, 2005. ICC 2005. 2005*, volume 2, pp. 1102–1106. IEEE, 2005.
- Greenfeld, D. and Shalit, U. Robust learning with the hilbert-schmidt independence criterion. In *International Conference on Machine Learning (ICML)*, 2020.
- Gretton, A., Bousquet, O., Smola, A., and Schölkopf, B. Measuring statistical dependence with hilbert-schmidt norms. In *International conference on algorithmic learning theory*, pp. 63–77. Springer, 2005a.
- Gretton, A., Herbrich, R., Smola, A., Bousquet, O., Schölkopf, B., et al. Kernel methods for measuring independence. *Journal of Machine Learning Research (JMLR)*, 2005b.
- Grill, J.-B., Strub, F., Alché, F., Tallec, C., Richemond, P., Buchatskaya, E., Doersch, C., Avila Pires, B., Guo, Z., Gheshlaghi Azar, M., et al. Bootstrap your own latent—a new approach to self-supervised learning. *Advances in Neural Information Processing Systems (NeurIPS)*, 2020.
- HaoChen, J. Z., Wei, C., Gaidon, A., and Ma, T. Provable guarantees for self-supervised deep learning with spectral contrastive loss. *Advances in Neural Information Processing Systems (NeurIPS)*, 2021.
- He, K., Zhang, X., Ren, S., and Sun, J. Deep residual learning for image recognition. In *Proceedings of the IEEE conference on computer vision and pattern recognition*, pp. 770–778, 2016.
- He, K., Chen, X., Xie, S., Li, Y., Dollár, P., and Girshick, R. Masked autoencoders are scalable vision learners. *arXiv preprint arXiv:2111.06377*, 2021.
- Hua, T., Wang, W., Xue, Z., Ren, S., Wang, Y., and Zhao, H. On feature decorrelation in self-supervised learning. In *Proceedings of the IEEE/CVF International Conference on Computer Vision*, pp. 9598–9608, 2021.
- Huang, L., Yang, D., Lang, B., and Deng, J. Decorrelated batch normalization. In *Proceedings of the IEEE Conference on Computer Vision and Pattern Recognition*, pp. 791–800, 2018.
- Huang, W., Yi, M., and Zhao, X. Towards the generalization of contrastive self-supervised learning. *arXiv preprint arXiv:2111.00743*, 2021.
- Husain, S. S. and Bober, M. Remap: Multi-layer entropy-guided pooling of dense cnn features for image retrieval. *IEEE Transactions on Image Processing*, 28(10):5201–5213, 2019.
- Hyvärinen, A. and Oja, E. Independent component analysis: algorithms and applications. *Neural networks*, 13(4-5): 411–430, 2000.
- Jacot, A., Gabriel, F., and Hongler, C. Neural tangent kernel: Convergence and generalization in neural networks. *Advances in neural information processing systems*, 31, 2018.
- Jing, L., Vincent, P., LeCun, Y., and Tian, Y. Understanding dimensional collapse in contrastive self-supervised learning. *arXiv preprint arXiv:2110.09348*, 2021.
- Kabal, P. Tsp speech database, 2002. McGill University, Database Version, 1(0):09-02.
- Kornblith, S., Norouzi, M., Lee, H., and Hinton, G. Similarity of neural network representations revisited. In *International Conference on Machine Learning (ICML)*, 2019.
- Leurgans, S. E., Moyeed, R. A., and Silverman, B. W. Canonical correlation analysis when the data are curves. *Journal of the Royal Statistical Society: Series B (Methodological)*, 55(3):725–740, 1993.
- Li, Y., Pogodin, R., Sutherland, D. J., and Gretton, A. Self-supervised learning with kernel dependence maximization. *Advances in Neural Information Processing Systems (NeurIPS)*, 2021.
- Li, Z., Tang, Y., Li, W., and He, Y. Learning disentangled representation with pairwise independence. In *Proceedings of the AAAI conference on artificial intelligence*, 2019.
- Melnick, E. L. and Tenenbein, A. Misspecifications of the normal distribution. *The American Statistician*, 36(4): 372–373, 1982.
- Micchelli, C. A., Xu, Y., and Zhang, H. Universal kernels. *Journal of Machine Learning Research (JMLR)*, 2006.
- Misra, I. and Maaten, L. v. d. Self-supervised learning of pretext-invariant representations. In *Proceedings of the IEEE/CVF Conference on Computer Vision and Pattern Recognition*, pp. 6707–6717, 2020.
- Mooij, J., Janzing, D., Peters, J., and Schölkopf, B. Regression by dependence minimization and its application to causal inference in additive noise models. In *International Conference on Machine Learning (ICML)*, 2009.
- Mourier, E. Eléments aléatoires dans un espace de banach. In *Annales de l’institut Henri Poincaré*, volume 13(3), pp. 161–244, 1953.

- Pfister, N., Bühlmann, P., Schölkopf, B., and Peters, J. Kernel-based tests for joint independence. *Journal of the Royal Statistical Society: Series B (Statistical Methodology)*, 80(1):5–31, 2018.
- Rahimi, A. and Recht, B. Random features for large-scale kernel machines. *Advances in Neural Information Processing Systems (NeurIPS)*, 2007.
- Rényi, A. On measures of dependence. *Acta mathematica hungarica*, 10(3-4):441–451, 1959.
- Schmidhuber, J. Learning factorial codes by predictability minimization. *Neural computation*, 4(6):863–879, 1992.
- Smola, A., Gretton, A., Song, L., and Schölkopf, B. A hilbert space embedding for distributions. In *International Conference on Algorithmic Learning Theory*, pp. 13–31. Springer, 2007.
- Steinwart, I. On the influence of the kernel on the consistency of support vector machines. *Journal of Machine Learning Research (JMLR)*, 2001.
- Sun, Y., Gilbert, A., and Tewari, A. On the approximation properties of random relu features. *arXiv preprint arXiv:1810.04374*, 2018.
- Taleb, A. and Jutten, C. Source separation in post-nonlinear mixtures. *IEEE Transactions on signal Processing*, 47(10):2807–2820, 1999.
- Tian, Y., Sun, C., Poole, B., Krishnan, D., Schmid, C., and Isola, P. What makes for good views for contrastive learning? *Advances in Neural Information Processing Systems (NeurIPS)*, 2020.
- Träuble, F., Creager, E., Kilbertus, N., Locatello, F., Dittadi, A., Goyal, A., Schölkopf, B., and Bauer, S. On disentangled representations learned from correlated data. In *International Conference on Machine Learning (ICML)*, 2021.
- Tsai, Y.-H. H., Bai, S., Morency, L.-P., and Salakhutdinov, R. A note on connecting barlow twins with negative-sample-free contrastive learning, 2021.
- Wang, F. and Liu, H. Understanding the behaviour of contrastive loss. In *Proceedings of the Conference on Computer Vision and Pattern Recognition (CVPR)*, 2021.
- Wang, T. and Isola, P. Understanding contrastive representation learning through alignment and uniformity on the hypersphere. In *International Conference on Machine Learning*, pp. 9929–9939. PMLR, 2020.
- Wightman, R., Touvron, H., and Jégou, H. Resnet strikes back: An improved training procedure in timm. *arXiv preprint arXiv:2110.00476*, 2021.
- Zaheer, M., Kottur, S., Ravanbakhsh, S., Poczos, B., Salakhutdinov, R. R., and Smola, A. J. Deep sets. *Advances in Neural Information Processing Systems (NeurIPS)*, 2017.
- Zbontar, J., Jing, L., Misra, I., LeCun, Y., and Deny, S. Barlow twins: Self-supervised learning via redundancy reduction. *arXiv preprint arXiv:2103.03230*, 2021.

A. Further Background

A.1. VCReg methods

Learning visual representations has a long history in machine learning. Shortly after the advent of convolutional neural networks (CNN), it was common to train a model on a supervised task such as ImageNet before removing the classifier and use the remaining model to produce features for downstream tasks (e.g., classification, segmentation), a technique coined transfer learning. Then, strategies to learn representations without labelled dataset by enforcing invariant embeddings for different versions of the same sample emerged (Misra & Maaten, 2020; Chen et al., 2020), hence the term “joint embedding”. Joint embedding methods can be divided in two categories. Contrastive learning (e.g., SimCLR (Chen et al., 2020)) pulls together representations of two augmented versions of the same image while pushing away the representation of this image from the representation of different images. Non-contrastive learning (e.g., DINO (Caron et al., 2021)) pulls together representations of two augmented versions of the same image while avoiding collapse using different techniques. The frameworks considered in this work belong to the latter category. Non-contrastive self-supervised representation learning of images has a few peculiarities:

- Data augmentations are central, at least when it comes to learn from ImageNet, and must be carefully chosen.
- Most methods are typically used either with Vision Transformers (Dosovitskiy et al., 2020), or with CNNs such as ResNets (He et al., 2016). In this work, we focus on ResNets.
- Model selection is usually performed via the Top1 accuracy on the validation set of ImageNet using a linear classifier on top of the learned representation. Outside of joint embedding, methods such as Masked-Auto-Encoder (He et al., 2021) perform poorly in linear evaluation while delivering excellent performance when fine-tuned on the downstream task.

The crucial role of the projector. It was found by (Chen et al., 2020) that adding a MLP on top of the encoder (removed after the training) significantly improved the quality of the learned representation. For example, in 100 epochs, VICReg without projector would achieve 48% validation accuracy on ImageNet instead of 68 and SimCLR 50% instead of 68%. Since then, a few theoretical work attempted to explain SSL with joint embeddings. (Jing et al., 2021) study the role of linear projectors with restricted augmentations, while other works such as (Huang et al., 2021; Wang & Isola, 2020; HaoChen et al., 2021; Tian et al., 2020; Wang & Liu, 2021) only consider an encoder without projector in their theoretical analysis. Finally, (Cosentino et al., 2022) consider a MLP projector in a very restricted context where data augmentations are Lie group transformations.

BarlowTwins. Zbontar et al. (2021) propose a slightly different approach based on regularizing C , the $P \times P$ cross-correlation matrix between Z_{left} and Z_{right} by optimizing

$$\mathcal{L}_{\text{BT}} = \sum_{k=1}^K ((C)_{k,k} - 1)^2 + \alpha \sum_{k' \neq k} (C)_{k,k'}^2. \quad (7)$$

Here, the leftmost term corresponds to regularizing the cross-correlation of the same feature in the two views to be unit, while the rightmost term regularizes the cross-correlation between pairs of different features in the two views. Importantly, $(C)_{i,j}$ falls back to measuring the cosine similarity between the i^{th} column of Z_{left} and the j^{th} column of Z_{right} i.e. $(C)_{i,j} = \frac{\langle (Z_{\text{left}})_{:,i}, (Z_{\text{right}})_{:,j} \rangle}{\|(Z_{\text{left}})_{:,i}\|_2 \|(Z_{\text{right}})_{:,j}\|_2}$. Hence, the leftmost term is also an invariance term: all features must be similar for both views.

W-MSE. Ermolov et al. (2021) use the following loss

$$\begin{aligned} \min 2 - 2 \frac{\langle Z_{\text{left}}, Z_{\text{right}} \rangle}{\|Z_{\text{left}}\|_2 \|Z_{\text{right}}\|_2} \\ \text{s.t. } \text{Cov}(Z_{\text{left}}) = Id, \text{Cov}(Z_{\text{right}}) = Id. \end{aligned}$$

where the cosine similarity can be replaced by the Euclidean distance.

A.2. Independent Component Analysis

The goal of ICA (Comon, 1994) is to find a transformation of a random vector \mathbf{Y}^2 which minimizes the statistical dependence of its components. Its simplest instance is linear ICA, and is motivated by problems such as the cocktail-party, where $\mathbf{Y} \in \mathbb{R}^{N \times D}$ typically results from a linear transformation of independent sources \mathbf{S} (e.g overlapping voices) one wants to recover. Formally, $\mathbf{Y} = \mathbf{S}\mathbf{A}$, with $\mathbf{A} \in \mathbb{R}^{D \times D}$ an unknown mixing matrix that can therefore not be inverted. Instead, the linear ICA approach searches for $\mathbf{M} \in \mathbb{R}^{D \times D}$ such that $\mathbf{Y}\mathbf{M} = \mathbf{S}$ by maximizing the statistical *mutual* independence between the components of $\mathbf{Y}\mathbf{M}$. Being able to recover \mathbf{S} is a property known as identifiability.

B. Proofs

B.1. Proof of Lemma 3.3: Random Linear Projectors maximize pairwise independence

Proof. Let's consider the linear regime for which $g((\mathbf{X})_{:,i}) = (\mathbf{X})_{:,i}\mathbf{w}_i^T$ with orthogonal weights i.e. $\langle \mathbf{w}_i, \mathbf{w}_j \rangle = 1_{\{i=j\}}$. This assumption is realistic since we assume that $\mathbf{w} \in \mathbb{R}^K$ with K very large, and that those are randomly sampled. From that, we then have

$$\begin{aligned} \sum_{i \neq j} \text{HSIC}((\mathbf{X})_{:,i}, (\mathbf{X})_{:,j}) &= \frac{1}{(N-1)^2} \sum_{i \neq j} \text{Tr}(g((\mathbf{X})_{:,i})g((\mathbf{X})_{:,i})^T \mathbf{H} g((\mathbf{X})_{:,j})g((\mathbf{X})_{:,j})^T \mathbf{H}) \\ &= \frac{1}{(N-1)^2} \sum_{i \neq j} \|g((\mathbf{X})_{:,i})^T \mathbf{H} g((\mathbf{X})_{:,j})\|_F^2, \end{aligned}$$

we will now push the sum inside the norm by considering the following equality:

$$\left\| \sum_{i \neq j} f(i, j) \right\|_F^2 = \sum_{i \neq j} \|f(i, j)\|_F^2 + \sum_{i \neq j} \sum_{k \neq \ell, (i,j) \neq (k,\ell)} \text{Tr}(f(i, j)^T f(k, \ell)) = \sum_{i \neq j} \|f(i, j)\|_F^2,$$

since in our case

$$\begin{aligned} f(i, j) &= g((\mathbf{X})_{:,i})^T \mathbf{H} g((\mathbf{X})_{:,j}) = \mathbf{w}_i(\mathbf{X})_{:,i}^T \mathbf{H}(\mathbf{X})_{:,j} \mathbf{w}_j^T, \\ f(i, j)^T f(k, \ell) &= \mathbf{w}_j(\mathbf{X})_{:,j}^T \mathbf{H}(\mathbf{X})_{:,i} \mathbf{w}_i^T \mathbf{w}_k(\mathbf{X})_{:,k}^T \mathbf{H}(\mathbf{X})_{:, \ell} \mathbf{w}_\ell^T, \\ \text{Tr}(f(i, j)^T f(k, \ell)) &= 1_{\{i=k \wedge j=\ell\}} (\mathbf{X})_{:,j}^T \mathbf{H}(\mathbf{X})_{:,i} (\mathbf{X})_{:,i}^T \mathbf{H}(\mathbf{X})_{:, \ell}, \end{aligned}$$

leading to

$$\begin{aligned} \sum_{i \neq j} \text{HSIC}((\mathbf{X})_{:,i}, (\mathbf{X})_{:,j}) &= \frac{1}{(N-1)^2} \left\| \sum_{i \neq j} g((\mathbf{X})_{:,i})^T \mathbf{H} g((\mathbf{X})_{:,j}) \right\|_F^2 \\ &= \frac{1}{(N-1)^2} \left\| \left(\sum_i g((\mathbf{X})_{:,i})^T \mathbf{H} \left(\sum_j g((\mathbf{X})_{:,j}) \right) - \sum_i g((\mathbf{X})_{:,i})^T \mathbf{H} g((\mathbf{X})_{:,i}) \right) \right\|_F^2 \\ &= \left\| \frac{1}{N-1} \left(\sum_i g((\mathbf{X})_{:,i})^T \mathbf{H} \left(\sum_j g((\mathbf{X})_{:,j}) \right) - \text{diag}(\text{Cov}(\mathbf{X}\mathbf{W})) \right) \right\|_F^2 \\ &= \left\| \text{Cov}(\mathbf{X}\mathbf{W}) - \text{diag}(\text{Cov}(\mathbf{X}\mathbf{W})) \right\|_F^2 \\ &= \sum_{i \neq j} \text{Cov}(\mathbf{X}\mathbf{W})_{i,j}^2, \end{aligned}$$

since we assume that all columns of \mathbf{X} have same variance and that \mathbf{W} is orthogonal we have for the pre-last equality

$$\frac{1}{N-1} \sum_i g((\mathbf{X})_{:,i})^T \mathbf{H} g((\mathbf{X})_{:,i}) = \text{Var}((\mathbf{X})_{:,1}) \sum_i \mathbf{w}_i \mathbf{w}_i^T = \text{Var}((\mathbf{X})_{:,1}),$$

and for the last equality we use the fact that since g is linear, $\sum_i g((\mathbf{X})_{:,i}) = \sum_i (\mathbf{X})_{:,i} \mathbf{w}_i^T = \mathbf{X}\mathbf{W}$ with $\mathbf{W} = [\mathbf{w}_1, \dots, \mathbf{w}_K]^T$.

□

²For simplicity, \mathbf{Y} directly denotes N empirical D -dimensional observations.

B.2. On the equivalence between VICReg and BarlowTwins objectives

We can express Barlow Twins objective as:

$$\begin{aligned} \min \sum_{k=1}^K (\text{Cov}(\mathbf{Z}_{\text{left}}, \mathbf{Z}_{\text{right}})_{k,k} - 1)^2 + \alpha \sum_{k' \neq k} \text{Cov}(\mathbf{Z}_{\text{left}}, \mathbf{Z}_{\text{right}})_{k,k'}^2 \\ \text{s.t. } \text{Cov}(\mathbf{Z}_{\text{left}}) = \mathbf{I}, \text{Cov}(\mathbf{Z}_{\text{right}}) = \mathbf{I}. \end{aligned}$$

Assuming $\mathbf{Z}_{\text{left}}^T \mathbf{Z}_{\text{left}} = \mathbf{I}$, $\mathbf{Z}_{\text{right}}^T \mathbf{Z}_{\text{right}} = \mathbf{I}$ i.e. perfect minimization of the variance and covariance terms, we have

$$C_{i,j} = \frac{\langle (\mathbf{Z}_{\text{left}})_{:,i}, (\mathbf{Z}_{\text{left}})_{:,j} \rangle}{\|(\mathbf{Z}_{\text{left}})_{:,i}\|_2 \|(\mathbf{Z}_{\text{left}})_{:,j}\|_2} = \frac{1}{2} \langle (\mathbf{Z}_{\text{left}})_{:,i}, (\mathbf{Z}_{\text{right}})_{:,j} \rangle = -\|(\mathbf{Z}_{\text{left}})_{:,i} - (\mathbf{Z}_{\text{right}})_{:,j}\|_2^2 - 1,$$

and thus

$$\sum_i (C_{i,i} - 1)^2 = \sum_i \|(\mathbf{Z}_{\text{left}})_{:,i} - (\mathbf{Z}_{\text{right}})_{:,i}\|_2^4 = \|\mathbf{Z}_{\text{left}} - \mathbf{Z}_{\text{right}}\|_F^4 \propto I(\mathbf{Z}_{\text{left}}, \mathbf{Z}_{\text{right}}),$$

so we recover the invariance loss exactly with the diagonal terms of BarlowTwins. We now show this is actually enough to minimize this quantity to also minimize the off-diagonal terms:

$$\begin{aligned} \sum_{i \neq j} C_{i,j}^2 &= \sum_{i \neq j} \left(1 - \frac{1}{2} \|(\mathbf{Z}_{\text{left}})_{:,i} - (\mathbf{Z}_{\text{right}})_{:,j}\|_2^2\right)^2 \\ &= \sum_{i \neq j} \left(1 - \frac{1}{2} \|(\mathbf{Z}_{\text{left}})_{:,i} - (\mathbf{Z}_{\text{left}})_{:,j} + (\mathbf{Z}_{\text{left}})_{:,j} - (\mathbf{Z}_{\text{right}})_{:,j}\|_2^2\right)^2 \\ &= \sum_{i \neq j} \left(1 - \frac{1}{2} \|(\mathbf{Z}_{\text{left}})_{:,i} - (\mathbf{Z}_{\text{left}})_{:,j}\|_2^2 - \frac{1}{2} \|(\mathbf{Z}_{\text{left}})_{:,j} - (\mathbf{Z}_{\text{right}})_{:,j}\|_2^2 \right. \\ &\quad \left. - \langle (\mathbf{Z}_{\text{left}})_{:,i} - (\mathbf{Z}_{\text{left}})_{:,j}, (\mathbf{Z}_{\text{left}})_{:,j} - (\mathbf{Z}_{\text{right}})_{:,j} \rangle\right)^2 \\ &= \sum_{i \neq j} \left(-\frac{1}{2} \|(\mathbf{Z}_{\text{left}})_{:,j} - (\mathbf{Z}_{\text{right}})_{:,j}\|_2^2 - \langle (\mathbf{Z}_{\text{left}})_{:,i} - (\mathbf{Z}_{\text{left}})_{:,j}, (\mathbf{Z}_{\text{left}})_{:,j} - (\mathbf{Z}_{\text{right}})_{:,j} \rangle\right)^2 \\ &= \sum_{i \neq j} \left(\frac{1}{2} \|(\mathbf{Z}_{\text{left}})_{:,j} - (\mathbf{Z}_{\text{right}})_{:,j}\|_2^2 + \langle (\mathbf{Z}_{\text{left}})_{:,i} - (\mathbf{Z}_{\text{left}})_{:,j}, (\mathbf{Z}_{\text{left}})_{:,j} - (\mathbf{Z}_{\text{right}})_{:,j} \rangle\right)^2 \\ &\leq \sum_{i \neq j} \left(\frac{1}{2} \|(\mathbf{Z}_{\text{left}})_{:,j} - (\mathbf{Z}_{\text{right}})_{:,j}\|_2^2 + \|(\mathbf{Z}_{\text{left}})_{:,i} - (\mathbf{Z}_{\text{left}})_{:,j}\|_2^2 \|(\mathbf{Z}_{\text{left}})_{:,j} - (\mathbf{Z}_{\text{right}})_{:,j}\|_2^2\right)^2 \\ &= \frac{25(K-1)}{4} \|\mathbf{Z}_{\text{left}} - \mathbf{Z}_{\text{right}}\|_2^4, \end{aligned}$$

hence minimizing the BarlowTwins loss with the explicit whitening constraint is equivalent to minimizing VICReg with explicit whitening constraint.

C. Additional experimental results

C.1. Illustrating Theorem 3.4

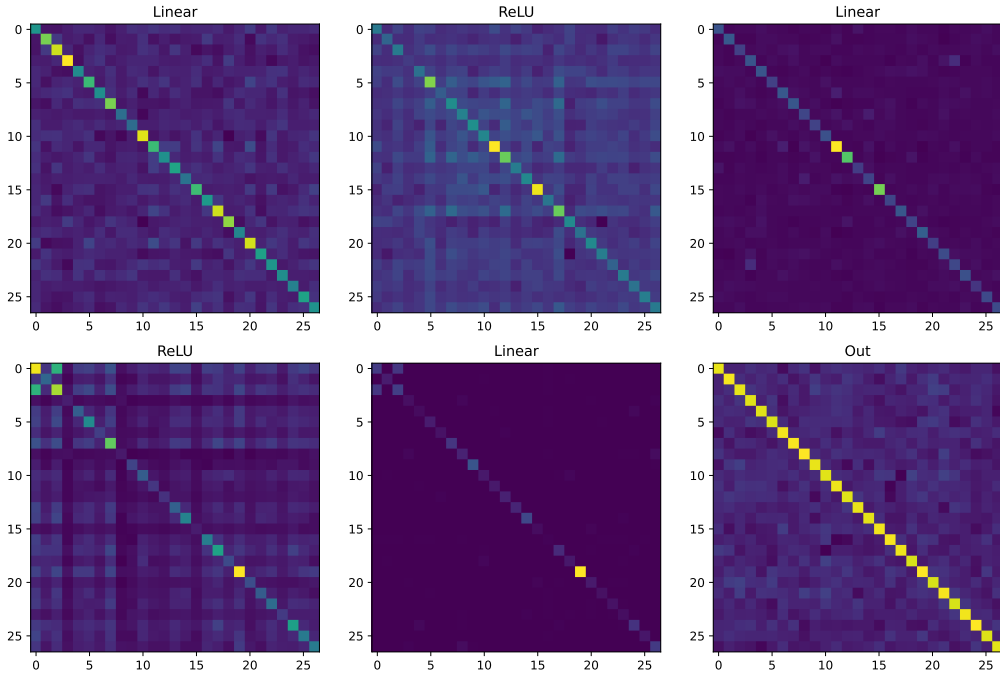


Figure 6. The covariance matrices for some features of each activation in a learned VICReg projector with width 8192 before corresponding hidden layer are close to diagonal, suggesting that each hidden layer output is implicitly VC-regularized.

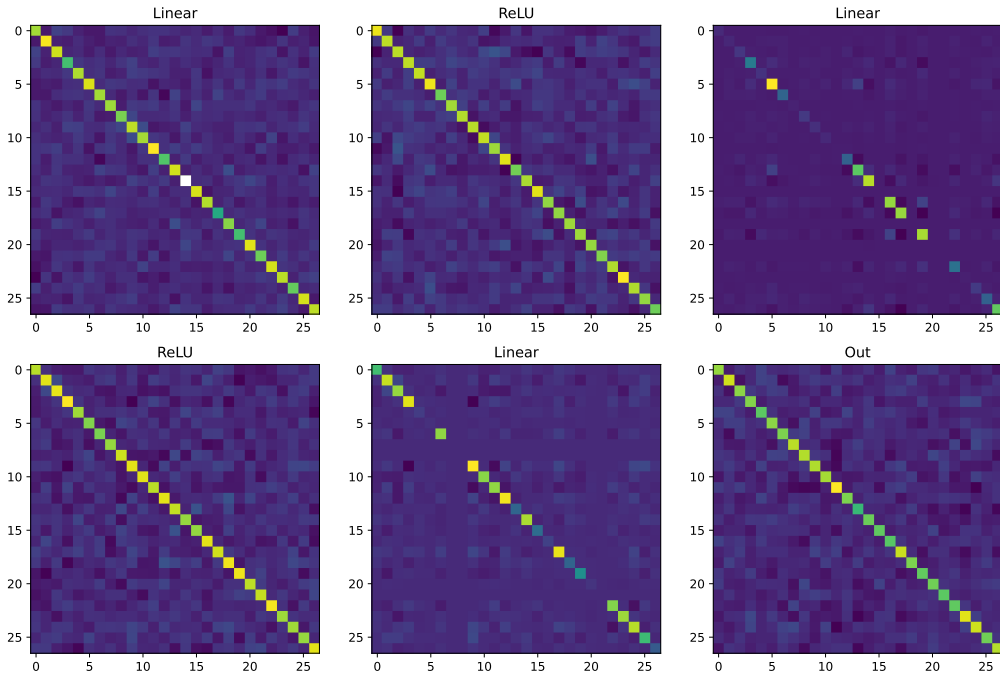


Figure 7. The covariance matrices for some features of each activation in a random VICReg projector (with width 8192) before corresponding hidden layer are close to diagonal, suggesting that each hidden layer output is implicitly VC-regularized.

C.2. Other factors of variation for HSIC

In this subsection, we illustrate the variation of HSIC induced by two more factors: varying the depth of the projector (Figure 8), and the covariance coefficient in VCREg (Table 4).

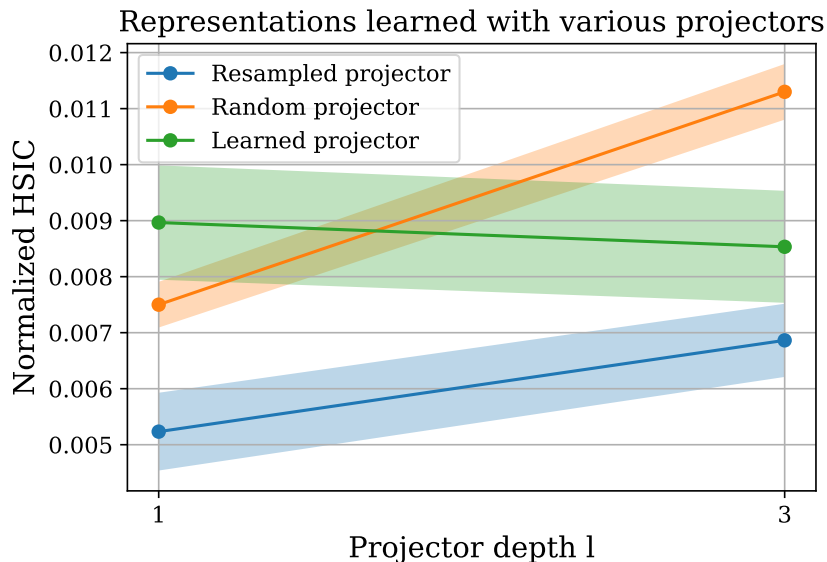


Figure 8. Increasing depth hurts HSIC for random projectors. Resampled projectors yield the representations with the lowest dependence amount.

Table 4. VCREg with a 512-512-512 projector and varying covariance coefficient. Increasing this coefficient decreases HSIC. Best accuracy does not always correspond to lowest Normalized HSIC: optimizing too much for Normalized HSIC is detrimental to the information content of the representation (it is trivial to train a representation too look pairwise independent. Doing so while extracting information from the input is harder).

Covariance coefficient in VCREg	1	2	4	8	16
Normalized HSIC (\downarrow)	0.017	0.0119	0.0090	0.0084	0.0084
Top1 ImageNet (\uparrow)	60.8	62.5	63.5	63.1	62.4

D. Implementations

D.1. HSIC Equation (2)

```

1 def GaussianKernelMatrix(X, sigma):
2     pairwise_distances = torch.cdist(X, X)
3     return torch.exp(-pairwise_distances / (2 * sigma**2))
4
5 def HSIC(X_1, X_2, sigma_1, sigma_2):
6     N = x.size(0) # batch size, should be the same for X_1 and X_2
7     K_1 = GaussianKernelMatrix(X_1, sigma_1) # Gaussian kernel matrix of X_1 with
8     bandwidth sigma_1
9     K_2 = GaussianKernelMatrix(X_2, sigma_2) # Gaussian kernel matrix of X_2 with
10    bandwidth sigma_2
11    H = torch.eye(N) - 1.0 / N # centering matrix
12    HSIC = torch.trace(K_1 @ H @ K_2 @ H) / ((N-1)**2)
13    return HSIC

```

In our study, the bandwidth σ of the Gaussian kernel is determined by the median of the distribution of pairwise euclidean distances between samples.

D.2. dHSIC Equation (4)

dHSIC can be estimated given empirical samples $\mathbf{X}_1, \dots, \mathbf{X}_d$ with respective kernel matrices $\mathbf{K}_1, \dots, \mathbf{K}_d$ as:

$$\text{dHSIC}(\mathbf{X}_1, \dots, \mathbf{X}_d) = \frac{1}{N^2} \sum_{i,j} (\odot_{k=1}^d \mathbf{K}_k)_{i,j} + \frac{1}{N^{2d}} \prod_{k=1}^d \sum_{i,j} (\mathbf{K}_k)_{i,j} - \frac{2}{N^{d+1}} \sum_i \odot_{k=1}^d \sum_j (\mathbf{K}_k)_{i,j}.$$

When $d = 2$, the first term corresponds to a biased HSIC estimator. The implementation of dHSIC is given by:

```

1 import GaussianKernelMatrix # defined above
2
3 def dHSIC(X, sigma):
4     length = X.shape(0)
5     term_1 = 1.0
6     term_2 = 1.0
7     term_3 = 2.0 / length
8     for j in range(D):
9         K_j = GaussianKernelMatrix(X[j])
10        term_1 = torch.mul(term_1, K_j)
11        term_2 = 1.0 / length / length / term_2 * torch.sum(K_j)
12        term_3 = 1.0 / length * term_3 * K_j.sum(axis=0)
13
14    term_1 = (1.0 / length) ** 2 * torch.sum(term_1)
15    term_3 = torch.sum(term_3)
16
17    return term_1 + term_2 - term_3 # the three terms of the estimator

```

As these evaluations already take a few minutes, scaling it to significantly larger portions of components would be impractical.

D.3. Linear ICA model 4

```

1 for p in projector.parameters(): # freeze the projector
2     p.requires_grad = False
3
4 for y in loader:
5     x = encoder(y) # matrix multiplication with M
6
7     z = projector(x) # compute embedding
8
9     C = torch.cov(z) # covariance matrix
10    loss = torch.MSE(C, torch.identity()) # VCReg loss
11    loss.backward()
12    optimizer.step()
13

```

```
14 projector.__init__() # to resample the projector
15 for p in projector.parameters(): # freeze the projector
16     p.requires_grad = False
```

D.4. Nonlinear ICA model 9

The implementation of our nonlinear ICA model 9 differs from 4 by the addition of a reconstruction constraint:

```
1 for p in projector.parameters(): # freeze the projector
2     p.requires_grad = False
3
4 for y in loader:
5     x = encoder(y) # MLP encoder
6
7     z = projector(x) # compute embedding
8
9     y_rec = reconstructor(x) # MLP reconstructor
10
11     C = torch.cov(z) # covariance matrix
12     loss = torch.MSE(C, torch.identity()) + lmda * torch.MSE(y, y_rec) # VCReg loss with
13     reconstruction
14     loss.backward()
15     optimizer.step()
16
17     projector.__init__() # to resample the projector
18     for p in projector.parameters(): # freeze the projector
19         p.requires_grad = False
```

E. Experimental details

E.1. Details on ImageNet experiments

Architectures and hyper-parameters. We use a Resnet50 bottleneck, optimized during 100 epochs with LARS and an initial learning rate of 0.3 for all methods. The batch size is 1024 for all methods except SimCLR. All methods have projector 8192 – 8192 – 8192 except DINO and Supervised. Throughout the training, we evaluate the learned representation using an online linear classifier. Details specific to each method:

- Barlow Twins: for Experiment 5.1, the off-diagonal coefficient is 0.0051.
- VICReg: for Experiment 5.1, the projector size is 8192 – 8192 – 8192, Invariance coeff is 25, Variance coeff is 25 and is Covariance coeff 1. For the rest of the experiments, and following (Bardes et al., 2022), we only move the covariance coefficient when changing the size of the projector. We scale it in the square root of the output size of the projector in order to have similar magnitude for the covariance term for all projector sizes.
- SimCLR: for Experiment 5.1, we choose a higher batch size of 2048 as SimCLR is sensitive to this parameter (Chen et al., 2020). The temperature is 0.15.
- DINO: we use 8 crops. The head has 4 layers of widths 2048 – 2048 – 2048 – 256 – 65536.

Augmentations. At train time, the resolution is 160 and we use

- `RandomHorizontalFlip()`.
- `ColorJitter(0.8, 0.4, 0.4, 0.2, 0.1)`.
- `Greyscale(0.2)`.
- `NormalizeImage` with ImageNet mean and standard deviation.
- `GaussianBlur()` with kernel size (5, 9) and sigma (0.1, 2).

At validation time, the resolution is 224 and the images are cropped and normalized with ImageNet mean and standard deviation.

E.2. ICA setup

Detailed setup. In these experiments, we keep the same optimizer, train on 100 epochs and choose a batch size of 64 for both datasets. We tune the learning rate according to a logarithmic grid [1.0, 10.0, 100.0] (then rescaled according to $\frac{lr \times batchsize}{256}$). The MLP can either be a SSL-like projector or simply a fully-connected layer followed by a ReLU. The wider the MLP, the better the result hence it does not require selection. For the synthetic dataset, the MLP has width 1024, and 8192 for the audio one.

- Linear ICA: We tune the standard and covariance coefficients according to a logarithmic grid [1, 10, 100].
- PNL ICA: Our architecture for the nonlinear ICA experiments is presented in Figure 9. The encoder f is a MLP with 3 layers and width 128. The decoder h is a learnable nonlinearity (a MLP with 3 hidden layers and depth 16) followed by a fully-connected layer. We tune the standard, covariance and reconstruction coefficients according to a larger logarithmic grid [1, 3, 10, 30, 100].

Reconstructed sources for ICA. In this paragraph, we provide ground truth sources for the synthetic data along with examples of reconstructed sources.

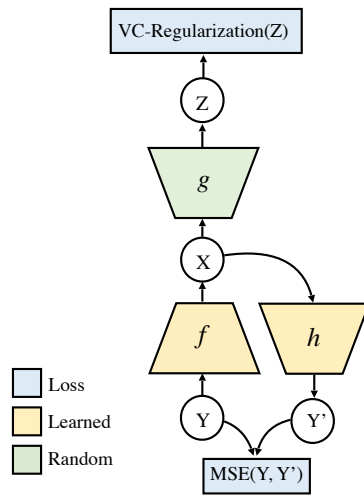


Figure 9. Nonlinear ICA model.

True sources

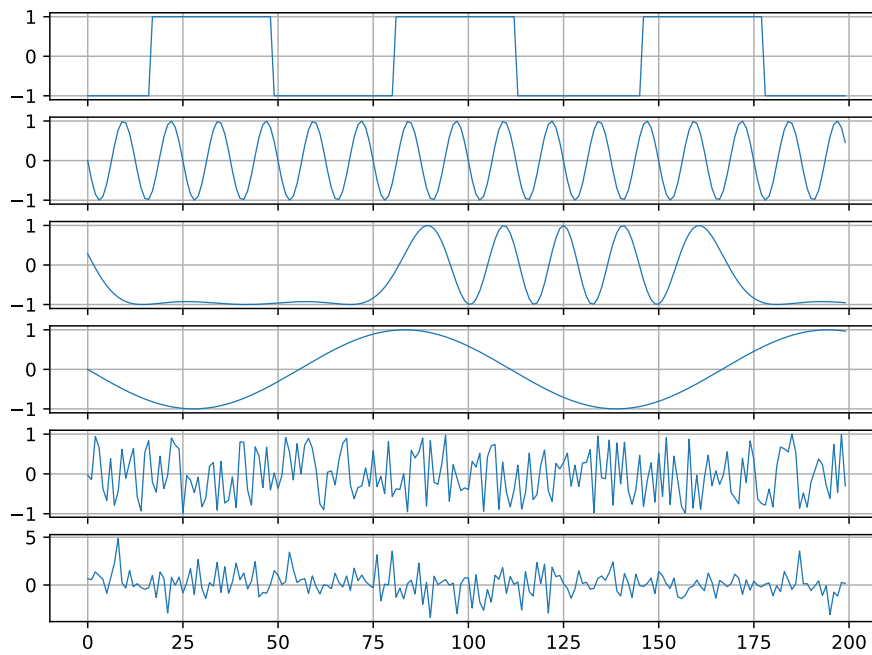


Figure 10. Data before mixing.

Mixed sources

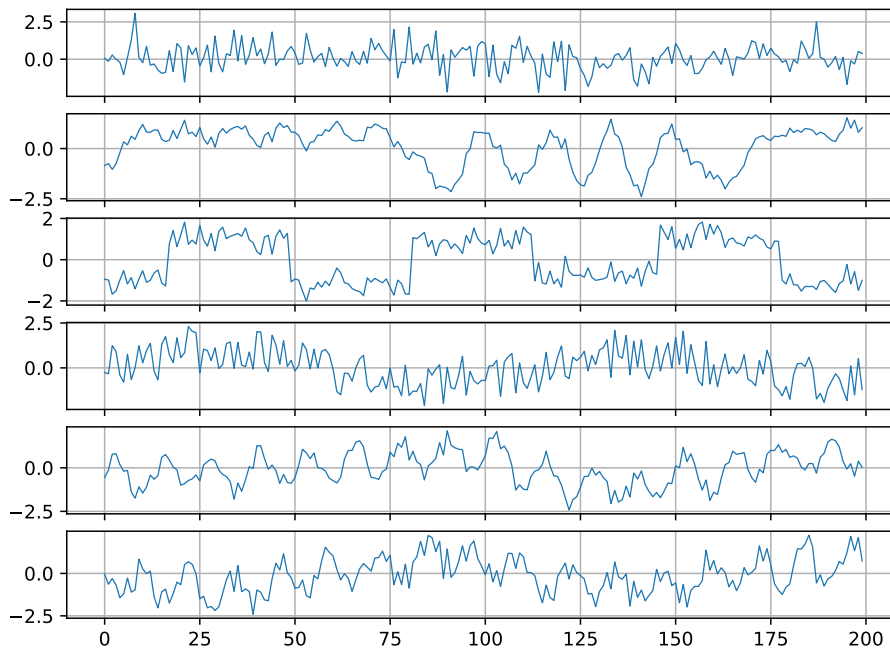


Figure 11. Data after mixing, before feeding to the various ICA models.

Reconstructed sources (max correlation=0.9996)

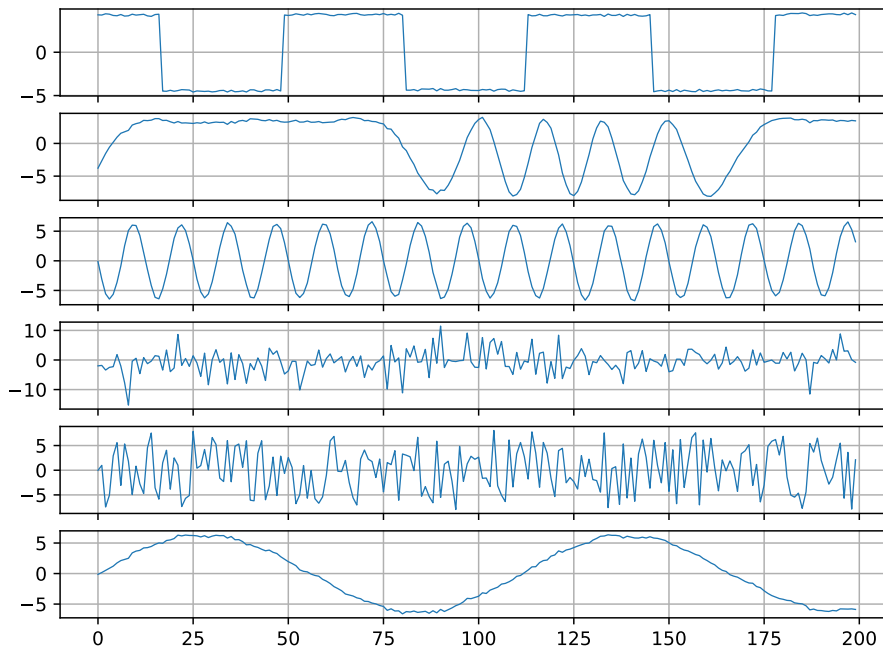


Figure 12. This level of max correlation is typically achieved by FastICA, VCReg or Anica.

Poorly reconstructed sources (max correlation = 0.8)

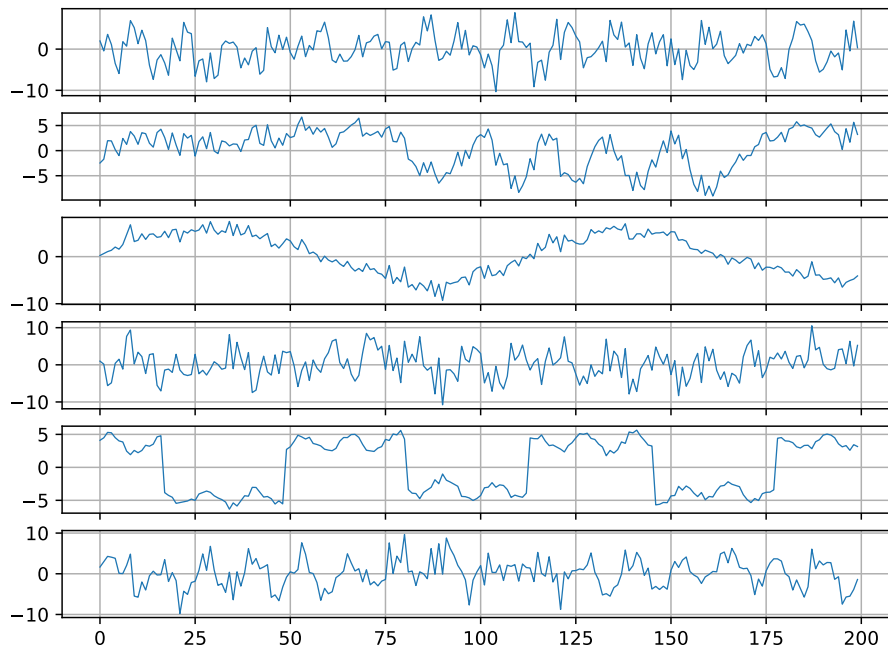


Figure 13. This level of max correlation is typically achieved by Whitening.